

The lowest doublet and quartet potential energy surfaces involved in the $N(^4S) + O_2$ reaction. II. *Ab initio* study of the C_{2v} -symmetry insertion mechanism

Miguel González,^{a)} Carolina Oliva, and R. Sayós^{a)}

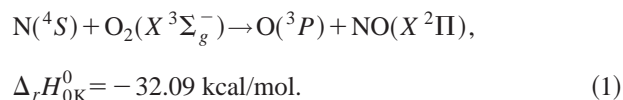
Departament de Química Física and Centre de Recerca en Química Teòrica, Universitat de Barcelona, C/Martí i Franquès 1, 08028 Barcelona, Spain

(Received 17 July 2001; accepted 18 April 2002)

In the present work we have carried out *ab initio* complete active space self-consistent field (CASSCF) and second-order perturbation theory on CASSCF wave function (CASPT2) calculations and also some density functional theory calculations with the aug-cc-pVTZ Dunning's basis set on the lowest A_1 , B_1 , A_2 , and B_2 doublet and quartet potential energy surfaces (PES) that could be involved in the title reaction. Thus, several minima, transition states, and surface crossings have been found for the C_{2v} -insertion reaction mechanism. The results agree very well with available experimental data [i.e., for $NO_2(^2A_1)$, $MIN2(^2B_2)$, $NO_2(^2\Pi_u)$] and with other previous *ab initio* calculations. Six A'/A' - and four A'/A'' -type surface crossings were located and classified for these PES', whose only one (i.e., $^2B_2/^2A_1$) has been previously reported in theoretical and experimental studies. High-energy barriers were found for the direct C_{2v} -insertion mechanism (3.11 and 2.54 eV for the lowest doublet and quartet PES' at the CASPT2/aug-cc-pVTZ level, respectively), clearly showing that this competitive mechanism is much less favorable than the direct C_s -abstraction or the indirect C_s -insertion reaction mechanisms reported in Paper I. © 2002 American Institute of Physics. [DOI: 10.1063/1.1484384]

I. INTRODUCTION

In a previous paper¹ (hereafter referred to as Paper I) we have described the C_s -symmetry direct abstraction and indirect insertion mechanisms for the following reaction:



In the present work we have studied the insertion of a nitrogen atom into the O_2 molecule preserving the C_{2v} symmetry. We have taken into account the lowest doublet and quartet A' (C_s -symmetry) potential energy surfaces (PES) involved in the title reaction. From these surfaces only one crossing between the C_{2v} PES' corresponding to the $NO_2(X^2A_1)$ and the $NO_2(A^2B_2)$ minima³⁻⁸ has been previously described. All the previous theoretical studies³⁻⁵ try to explain the extremely complex spectrum of NO_2 . From multireference configuration interaction (MR-CI)³ calculations coupling elements have been obtained, and with this information potential energy functions for the two lowest $^2A'$ NO_2 states, in both the diabatic and adiabatic representations, have been derived.^{4,5} Experimental studies of electron impact energy loss spectra of the $NO_2 A^2B_2 \leftarrow X^2A_1$ transition⁸ agree with the theoretical results for the transition vertical energy.⁴ The geometrical parameters obtained theoretically agree with those estimated from extrapolations of observed spectroscopic bands.^{6,7} In the above-mentioned theoretical studies,

both minima involved in the crossing [i.e., $NO_2(X^2A_1)$ and $NO_2(A^2B_2)$], and the $NO_2(^2\Pi_u)$ linear minimum have also been described. Some papers deal with the characterization of a great number of different NO_2 minima for the doublet surface^{9,10} and for the quartet one.⁹ In those papers, some intersections between different surfaces and the electronic configurations implicated were described. More recent calculations for the $NO_2(X^2A_1)$ minimum have been done at the CASSCF and CISD *ab initio* levels, where the energetic difference between the bend (X^2A_1) and linear ($^2\Pi_u$) minima was studied.¹¹ Some symmetry breaking studies for the NO_2 radical have also been done at the CASSCF¹² and MR-CCSD¹³ levels, where geometries and frequencies for the $NO_2(X^2A_1)$ and $NO_2(A^2B_2)$ minima were obtained. *Ab initio* studies of the peroxy and cyclic isomers of NO_2 and NO_2^- have been done, being the $NO_2(^2B_1)$ cyclic minimum described.¹⁴ In all previous theoretical works about the 2A_1 and 2B_2 surfaces, the nuclear regions explored correspond to ONO angles in the range 80° – 90° ; consequently, they are not able to describe the C_{2v} -symmetry insertion reaction mechanism coming from $N(^4S) + O_2(X^3\Sigma_g^-)$.

Crossings between surfaces of different electronic states can be important in different molecular processes. When there is a conical intersection between both PES', the excited state is funneled into the intersection region favoring its radiationless decay to the ground state.¹⁵ This is a direct effect¹⁶ because nuclear motion takes place on both surfaces, the ground one and the excited one, and is due to the PES topology of the excited state near the intersection. Another direct effect is the nonadiabatic recrossing,¹⁷ where the potential motion takes place on both surfaces but the overall

^{a)}Authors for correspondence. Electronic mail: miguel@qf.ub.es, r.sayos@qf.ub.es

process begins and ends on the same surface. In this case, due to derivative couplings, the nuclear motion cannot follow the adiabatic reactive path and follows a nonadiabatic nonreactive one, the intersection region being recrossed several times. This effect will be more important if the intersection point and the true saddle point connecting the two intersection regions are so close.¹⁸ An indirect effect, in which the nuclear motion only takes place on one potential energy surface, is produced by the geometric phase effect.¹⁹ Due to this effect the nuclear wave function transported around a conical intersection acquires a nondynamical or geometric phase, which is necessary to compensate the phase changes of the adiabatic electronic wave function. This effect could have important consequences in reaction dynamics because it can affect reaction probabilities (e.g., the H₃ system²⁰). The main point is that the conical intersection has not to be energetically accessible; only a closed loop around the conical intersection is necessary to be accessible itself. As a consequence, the effect of a conical intersection on reaction dynamics cannot be anticipated, taking into account only its energy. For all these reasons, conical intersections^{21–23} have to be thought as normal features on potential energy surfaces whose effects have to be taken into account.

We are particularly interested in the effects that these intersections could produce in the dynamics of the title reaction for electronically ground or excited reactants. Moreover, the characterization of these intersections can also help in the elucidation of the rather complicated spectra of the NO₂ molecule, and also in the construction of new analytical PES' (e.g., ²A' and ⁴A'), essential for accurate theoretical studies of the title reaction.

This work is organized as follows: the method of calculation is described in Sec. II, our results are presented in Sec. III, and in Sec. IV the concluding remarks are given.

II. THEORETICAL METHODS

The CASSCF method^{24,25} was used throughout this study, always choosing the lowest two roots in C_s symmetry for both the doublet and the quartet PES' (i.e., A' and A''), which were obtained using the two-state-averaged methodology.²⁶ Calculations in C_{2v} symmetry were also performed to locate the different intersections of the diabatic PES', in this case obtaining the first root of each symmetry (A₁, B₁, A₂, and B₂), with the exception of the I2 intersection, where we made calculations with the first and second roots due to the fact that this intersection implied two states of the same symmetry.

The full-valence active space comprising 17 electrons in 12 orbitals [i.e., CAS(17,12)] was applied in all calculations as in Paper I. The standard correlation-consistent aug-cc-pVTZ Dunning's basis set²⁷ was also used in the present study; this implies a total of 138 basis functions, 46 on each atom. The dynamical correlation was included by performing CASPT2 calculations using the G2 variant.²⁸ All the CASSCF and CASPT2 G2 calculations were done with the MOLCAS 4.1 program.²⁹

The location of stationary points [i.e., minima (MIN) and transition states (TS)] was achieved by employing ana-

lytic CASSCF gradients. The full characterization of them was effected by calculating the numerical Hessian matrix at the optimized geometries. Intrinsic reaction coordinate (IRC) and approximate minimum energy paths (MEP) calculations were also carried out to verify connections between the stationary points. In some cases, we have used the SURVIBTM program³⁰ to locate some stationary points using a grid of points previously calculated at the CASSCF or CASPT2 levels, following the same method described in Paper I.

In order to locate the intersections (I) we have fitted different regions of each diabatic surface using bicubic splines.³¹ Using these fittings we have calculated more points around the intersection regions and we have done the difference between both surfaces that were likely to intersect. Doing that, we were able to extract the seam of the conical intersection and to locate the minimum of this seam. We have studied the topology of the located intersections, which allows us to classify them. To do this, we have used the GAUSSIAN 98 program³² with a reduced active space CAS(7,6) and the 6-31G(d) Pople's basis set in order to identify the two coordinates that define a conical intersection.

In spite of a rigorous check of whether or not the intersection is of a conical type was not carried out, we will use through the paper this name indistinctly. An intersection is conical if the electronic wave function changes its sign when is transported around a closed loop that encircles the intersection. For this to occur it is necessary that the two conditions that have to be accomplished to find an intersection [$\Delta H(\mathbf{q}) = H_{AA}(\mathbf{q}) - H_{BB}(\mathbf{q}) = 0$ and $H_{AB}(\mathbf{q}) = 0$] were satisfied for all N values of the internal coordinates ($\mathbf{q} = q_1, q_2, \dots, q_N$) that describe the geometry of the nuclear arrangement. Sometimes the second condition is accomplished by symmetry (e.g., both states belong to different irreducible representations in C_{2v}) but not all C_{2v} geometries give rise to conical intersections.¹⁸

Apart from *ab initio* calculations we have also performed some density functional theory (DFT) calculations (i.e., UB3LYP/aug-cc-pVTZ) with a GAUSSIAN 98 code too, such as in Paper I, where we found a very similar and accurate description in comparison to the largest *ab initio* calculations.

Supermolecule calculations were considered in the determination of all energies in both the *ab initio* and the DFT calculations.

The present methodology has previously provided good results concerning the location of all stationary points on the ²A' and ⁴A' PES' (C_s geometries) involved in the N(⁴S) + O₂(X³Σ_g⁻) reaction,¹ in comparison with experimental data or larger calculations, and also in the study of similar reactions [e.g., N(²D) + NO³³ and N(²D) + O₂³⁴].

III. RESULTS AND DISCUSSION

A. Stationary points

The first step in our study was the search of the main C_{2v} stationary points belonging to ²B₂, ⁴B₂, ²A₁ and ⁴A₁ PES' to compare with available previous published data. We found several minima and transition states on these surfaces (i.e., ²A' and ⁴A' PES' in C_s symmetry), whose geometry,

TABLE I. *Ab initio* and DFT properties of several C_{2v} stationary points located on the doublet and quartet A' PES'.^a

	Method	Basis set	$R_{e(\text{NO})}/\text{Å}$	$\angle\text{ONO}^\circ$		ω_i/cm^{-1b}	$\Delta E/\text{eV}^c$	
TS1 (4A_1)	CASSCF(17,12)	aug-cc-pVTZ	1.7460	46.71	1013.83	674.40	2525.23i	6.77
	CASPT2(17,12) G2	"						6.79
	UB3LYP	"	1.7348	45.33	1182.19	672.00	2606.55i	6.63
TS2 (4A_1)	CASSCF(17,12)	"	1.3890	87.33	1126.00	588.93	464.91i	4.44
	CASPT2(17,12) G2	"	1.3682	84.78	1296.82	631.54	259.15i	4.38
	UB3LYP	"	1.3714	86.23	1197.43	657.17	337.59i	4.22
TS3 (2A_1)	CASSCF(17,12)	"	1.7848	46.18	965.56	640.35	2276.20i	7.19
	CASPT2(17,12) G2	"						7.27
	UB3LYP	"	1.7865	43.07	1223.71	537.12	3334.84i	7.07
$\text{NO}_2(^2A_1)$	CASSCF(17,12) ^d	"	1.2040	133.95	1335.76	753.15	1608.79	0.00
	CASPT2(17,12) G2	"	1.1965	134.30	1344.13	755.27	1677.17	0.00
	UB3LYP ^d	"	1.1912	134.45	1385.88	766.12	1688.07	0.00
	MR-CI ^e	[9s5p1d/5s3p1d]	1.206	133.4	0.00
	MR-CI/adiabatic potentials ^f	[9s5p1d/5s3p1d]	1.203	133.6	1360	829	1570	0.00
	CISD ^g	QZ+2P	1.174	135.1	1502	809	1821	0.00
	CASSCF(13,10) ^{g,h}	Huzinaga–Dunning DZ+P	1.219	133.0	1322	737	1631	0.00
	MR-CCSD ⁱ	Huzinaga–Dunning DZ+P	1.213	133.2	1380	737	1689	0.00
	experimental ^j		1.197	134.25	1357.8	756.8	1665.5	0.00
	MIN1 (4B_2)	CASSCF(17,12)	aug-cc-pVTZ	1.3117	124.17	1079.58	563.43	561.16i
CASPT2(17,12) G2		"	1.2952	124.60	1174.72	664.77	557.17	4.04
UB3LYP		"	1.2943	124.68	1152.67	590.89	456.04	3.75
MIN2 (2B_2)	CASSCF(17,12)	"	1.2690	101.73	1389.45	741.36	181.28	1.16
	CASPT2(17,12) G2	"	1.2584	102.06	1390.93	952.77	777.51	1.31
	UB3LYP	"	1.2521	101.77	1459.29	767.85	671.99	1.40
	CASSCF(13,10) ^h	Huzinaga–Dunning DZ+P	1.281	101.3	1391	730	359	1.06
	MR-CCSD ⁱ	Huzinaga–Dunning DZ+P	1.270	100.6	1480	758	792	1.05
	MR-CI adiabatic potentials ^f	[9s5p1d/5s3p1d]	1.277	101.9	1.08
	Experimental ^k		1.26	102	1.21
Experimental ^l		1470	745	1740	...	

^aThe CASPT2 G2 energies, geometries, and harmonic vibrational frequencies reported were derived from a grid of points by using the SURVBTM program (Ref. 30). In some cases only the CASPT2 energy at the CASSCF geometry is given.

^bHarmonic vibrational frequencies: ω_s (sym. str., a_1), ω_b (bend., a_1), and ω_a (asym. str., b_2), respectively (YZ taken as the molecular plane). Masses of the most abundant isotopes were used: ^{14}N and ^{16}O .

^cEnergy respect to $\text{NO}_2(X^2A_1)$.

^dReference 1. Dissociation energy to $\text{O}(^3P) + \text{NO}$: 49.05, 80.69, and 77.22 kcal/mol at CASSCF(17,12) CASPT2(17,12) G2, UB3LYP with the aug-cc-pVTZ basis set.

^eReference 3.

^fReference 4. A B_2 stationary point characterized as a saddle.

^gReference 11.

^hReference 12.

ⁱReference 13.

^jReference 2. Fundamental ν_i frequencies are reported. Dissociation energy to $\text{O}(^3P) + \text{NO}$ equal to 74.48 kcal/mol (Ref. 35).

^kReference 36.

^lReference 37.

harmonic frequencies and energy are shown in Table I. The most energetic ones correspond to TS in 2A_1 and 4A_1 PES', (i.e., TS3 and TS1, respectively). Neither these stationary points nor TS2 in 4A_1 and MIN1 in 4B_2 PES' have been described previously.

For $\text{NO}_2(^2A_1)$ molecule and MIN2, there are preceding theoretical and experimental data to compare with. The results presented in Table I at the highest *ab initio* level (i.e., CASPT2) are very close to the experimental ones and much better than the earlier theoretical studies. The exception is mainly the MIN2 asymmetric stretching harmonic frequency, which is difficult to calculate due to the closeness of a conical intersection. As there will be show later (Sec. III C), all TS are close to the crossings between PES' of A' or A'' symmetry.

TS1 connects two equivalent $\text{NOO}(^4A')$ peroxy minima ($R_{e(\text{NO})} = 1.3779 \text{ Å}$, $R_{e(\text{OO})} = 1.3546 \text{ Å}$, $\angle\text{NOO} = 102.73^\circ$ ΔE

$= 4.90 \text{ eV}$ at the same *ab initio* level) described in Paper I. TS3 probably connects also with two equivalent $\text{NOO}(^2A')$ peroxy minima described also in Paper I ($R_{e(\text{NO})} = 1.2170 \text{ Å}$, $R_{e(\text{OO})} = 1.3491 \text{ Å}$, $\angle\text{NOO} = 123.81^\circ$ $\Delta E = 3.73 \text{ eV}$ at the same *ab initio* level). TS2 is the transition state for the oxygen exchange reaction: $\text{O}(^3P) + \text{NO}' \rightarrow \text{NO} + \text{O}'(^3P)$, with an energy barrier of 0.85 eV respect this surface asymptote. The connectivity of these transition states was also confirmed by doing IRCs at the UB3LYP/aug-cc-pVTZ level, although for TS3 we were not able to do the IRC at this level due to the convergence problems originated by the spin contamination (i.e., $\langle S^2 \rangle$ was 1.78 to be compared with the correct expectation value of 0.75), which arises from the proximity of the quartet TS1.

MIN1 presents an imaginary frequency at the CASSCF level, but that disappears at CASPT2 G2 and UB3LYP lev-

TABLE II. *Ab initio* and DFT properties of several C_{2v} stationary points located on the doublet and quartet A'' PES'.^a

	Method	Basis set	$R_{e(\text{NO})}/\text{\AA}$	$\angle\text{ONO}/^\circ$	ω_i/cm^{-1b}	$\Delta E/\text{eV}^c$		
MIN3 (4A_2)	CASSCF(17,12)	aug-cc-pVTZ	1.3139	112.36	1105.90	525.89	682.45	3.70(3.66)
	UB3LYP	"	1.2932	113.55	1178.66	548.54	886.93	3.36
	CI ^d	[9s5p/4s2p]	1.328	115.2	2.58
MIN4 (2A_2)	CASSCF(17,12)	aug-cc-pVTZ	1.5784	48.99	1211.79	750.75	1028.44	5.79(6.08)
	UB3LYP	"	1.5549	49.06	1303.29	835.09	1028.95	5.96
MIN5 (2B_1)	CASSCF(17,12)	"	1.3813	67.44	1218.60	736.68	668.63	3.27(3.49)
	UB3LYP	"	1.3680	66.06	1294.54	845.30	644.15	3.51
	CASSCF(17,12) ^e	[9s5p1d/4s2p1d]	1.388	67.5	1223	720	691	2.91
	CISD ^e	[11s7p2d/6s4p2d]	1.349	65.8	1363	873	716	3.38
	CI ^d	[9s5p/4s2p]	~1.40	~75	2.98

^aCASPT2(17,12) G2 energies at CASSCF geometries are given between parentheses.

^bHarmonic vibrational frequencies: ω_s (sym. str., a_1), ω_b (bend., a_1), and ω_a (asym. str., b_2), respectively (YZ taken as the molecular plane). Masses of the most abundant isotopes were used: ^{14}N and ^{16}O .

^cEnergy respect to $\text{NO}_2(X^2A_1)$.

^dReference 10.

^eReference 14. The energy at the CISD+Q level is equal to 3.32 eV.

els. The imaginary frequency found at the CASSCF level corresponds to the asymmetric stretching mode. This fact means that this stationary point is a saddle point and that the surface bifurcates at this point, thus MIN1 showing symmetry breaking only at the CASSCF level.

Table II presents the different minima found for the 2A_2 , 4A_2 and 2B_1 PES' (i.e., $^2A''$ and $^4A''$ PES' in C_s symmetry). Minima 4 and 5 have a rather cyclical structure. The calculated properties of the cyclic 2B_1 isomer (MIN5) are reasonably consistent at both levels of theory and also with theoretical earlier predictions. Another open minimum in the 2A_2 PES was also located [$R_{e(\text{NO})}=1.2855 \text{\AA}$, $\angle\text{ONO}=110.00^\circ$, $\Delta E=1.86$ (2.31) eV at the same *ab initio* level as shown in Table II], although more details and a comparison with experimental and other theoretical studies will be reported in a paper in progress about the excited A'' PES. The most stable angular minima found are the MIN2(2B_2) and the MIN3(4A_2) for the doublet and quartet cases apart from the $\text{NO}_2(^2A_1)$ molecule.

We have also studied the linear $\text{NO}_2(^2\Pi_u)$ stationary point (Table III). At this geometrical configuration the 2A_1 and the 2B_1 states become degenerated, as has been previously shown.^{3-5,11} Upon bending the $^2\Pi_u$ state splits into the

$^2A_1-^2B_1$ pair via a Renner-Teller mechanism.⁴⁰ Its strong interaction produces an upper state with a linear conformation and a lower state with a bent one.¹⁰ The calculated energies and geometries (Table III) agree very well with the experimental values and with another published *ab initio* data. This structure is characterized as a minimum in the 2B_1 surface and as a transition state in the lower 2A_1 surface at its equilibrium geometry, as it is shown in Table III.

In order to understand how these stationary points could affect the reactivity we have approximately derived MEPs (Figs. 1 and 2) from grids of *ab initio* points, by using as the reaction coordinate a combination of the distance from the N atom to the center of mass of the diatomic OO molecule (R) and the diatomic OO distance (r). At the beginning of the C_{2v} insertion approach the reaction coordinate is practically equal to the R distance and at the end it coincides approximately with the r distance, but for middle configurations both coordinates become important (r and R). In C_{2v} symmetry the $\text{N}(^4S)+\text{O}_2(X^3\Sigma_g^-)$ reactants correlate with 2,4B_2 PES' and the $\text{O}(^3P)+\text{NO}(X^2\Pi)$ products with $2(^2,4A_1)$, $2(^2,4B_1)$, 2,4B_2 and 2,4A_2 PES'. This means that reactants and products can be connected through a B_2 PES in the doublet case and also in the quartet one. In the doublet case

TABLE III. *Ab initio* and DFT properties of the linear $\text{NO}_2(^2\Pi_u)$ structure.^a

	Method	Basis set	$R_{e(\text{NO})}/\text{\AA}$	ω_i/cm^{-1b}	$\Delta E/\text{eV}^c$		
$\text{NO}_2(^2\Pi_u)$	CASSCF(17,12)	aug-cc-pVTZ	1.2084	1135.13	1424.71i ^d	1848.91	1.79(1.74)
	UB3LYP	"	1.1959	1191.85	1299.85i	1927.46	1.62
	MR-CI ^e	[9s5p1d/5s3p1d]	1.206	1.91
	CISD ^f	QZ+2P	1.182	1266	1417i	1961	1.74
	MR-CI/adiabatic potentials ^g	[9s5p1d/5s3p1d]	1.203	1.85
	Experimental ^h			1.23

^aCASPT2(17,12) G2 energies at CASSCF geometries are given between parentheses.

^bHarmonic vibrational frequencies: ω_s (sym. str., Σ_g^+), ω_b (bend., Π_u), and ω_a (asym. str., Σ_u^+), respectively (YZ taken as the molecular plane). Masses of the most abundant isotopes were used: ^{14}N and ^{16}O .

^cEnergy with respect to $\text{NO}_2(X^2A_1)$.

^dFrequencies calculated as a minimum in the upper 2B_1 PES: 1135.42 (Σ_g^+) 463.20 (Π_u), and 1848.82 (Σ_u^+) cm^{-1} , respectively.

^eReference 3.

^fReference 11.

^gReference 4.

^hReferences 38-39.

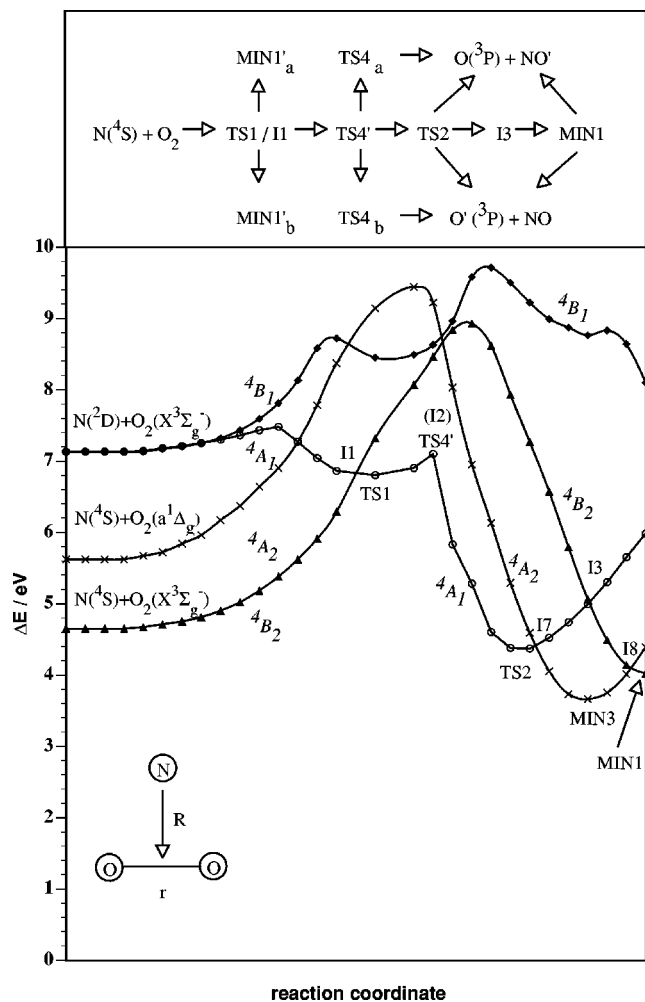


FIG. 1. Approximate $N+O_2$ C_{2v} MEPs for quartet PES' at the CASPT2 G2/aug-cc-pVTZ level. Zero of energy in the NO_2 (X^2A_1) molecule. The point indicated here as (I2) corresponds to an avoided crossing, where the separation between both 4A_1 surfaces is higher than at the I2 intersection (the point of closest approach). At the top there is one scheme with the main stationary points and surface intersections involved in the C_{2v} MEP (C_s distortions are indicated out of the central line) for the lowest adiabatic $^4A'$ PES. Subscripts **a** and **b** are used to distinguish between the equivalent NOO' and $NO'O$ structures.

the ground surface 2B_2 arising from reactants can cross with the other PES' of different symmetries (A_1 , A_2 , or B_1), which correlate with $N(^2D)+O_2$ ($X^3\Sigma_g^-$) reactants, 2.48 eV above ground state reactants at the CASPT2 G2/aug-cc-pVTZ level (the experimental value is 2.38 eV²). For the quartet PES' there exists an important difference due to the fact that the 4A_2 surface correlates now with $N(^4S)+O_2$ ($a^1\Delta_g$), 1.04 eV above ground state reactants at the CASPT2 G2/aug-cc-pVTZ level (the experimental value is 0.98 eV²), instead of $N(^2D)+O_2$ ($X^3\Sigma_g^-$) reactants. These electronic correlations help us to understand the asymptotic regions shown in Figs. 1 and 2, where there are also depicted two schemes summarizing the main stationary points and surface intersections involved in the C_{2v} regions of the lowest $^2A'$ and $^4A'$ PES', and hence relevant for the C_{2v} - $N(^4S)+O_2$ ($X^3\Sigma_g^-$) insertion reaction mechanism. We

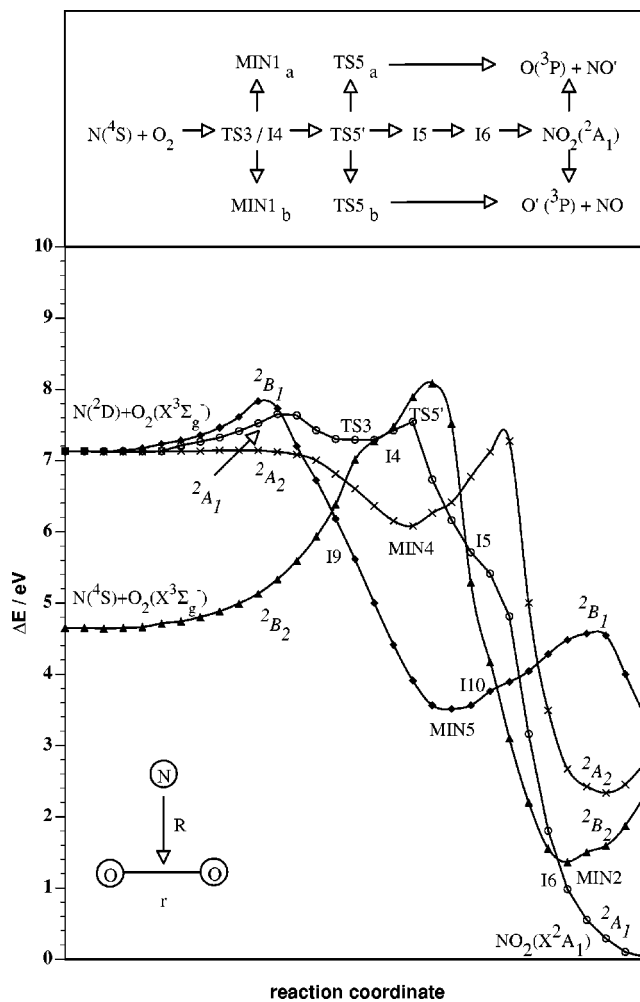


FIG. 2. Approximate $N+O_2$ C_{2v} MEPs for doublet PES' at the CASPT2 G2/aug-cc-pVTZ level. Zero of energy in the NO_2 (X^2A_1) molecule. At the top there is one scheme with the main stationary points and surface intersections involved in the C_{2v} MEP (C_s distortions are indicated out of the central line) for the lowest adiabatic $^2A'$ PES. Subscripts **a** and **b** are used to distinguish between the equivalent NOO' and $NO'O$ structures.

can see that this C_{2v} insertion reaction path (or with a C_s -symmetry approach close to C_{2v} symmetry) shows very high-energy barriers on both surfaces [2.54 and 2.13 eV for the $^2A'$ (TS5) and $^4A'$ (TS4) PES' at the CASPT2 G2/aug-cc-pVTZ level, respectively], but lower for the quartet surface. This behavior is just contrary to the one observed in the direct C_s -abstraction reaction mechanism studied in Paper I, where, in addition, much lower-energy barriers were reported for both PES' (0.20 and 0.55 eV, respectively, at the same *ab initio* level). Table IV summarizes the properties of both transition states. C_{2v} structures (TS4' and TS5') are second-order saddle points that connect with the true transition states (TS4 and TS5).

These latter results confirm that the direct C_{2v} insertion reaction pathway is much less favorable than the other competitive reaction pathways (e.g., C_s -symmetry abstraction and insertion mechanisms through the $^2A'$ PES) presented in Paper I.

TABLE IV. Transition States for the C_{2v}-insertion reaction mechanism through the doublet and quartet A' PES'.^a

Method	Basis set	R _{e(NO)} /Å	R _{e(NO)} /Å	<ONO/°	ω _i /cm ^{-1b}	ΔE/eV ^c
TS4' (⁴ A')	CASSCF(17,12)	aug-cc-pVTZ	1.6304	1.6304	55.88	1655.89i 734.73 771.28i 7.17(7.20)
TS4 (⁴ A')	"	"	1.6073	1.6698	50.33	1642.42i 1673.22 1524.93 6.79(6.79)
TS5' (² A')	"	"	1.6865	1.6865	55.05	1394.82i 558.60 870.74i 7.61(7.77)
TS5 (² A')	"	"	1.6199	1.7135	51.01	665.51i 1842.45 1350.01 7.08(7.20)

^aCASPT2(17,12) G2 energies at CASSCF geometries are given between parentheses. TS4' and TS5' are second-order saddle points that give place to true transition states TS4 and TS5 (i.e., first-order saddle points).

^bHarmonic vibrational frequencies: (a) C_{2v}: ω_s (sym. str., a₁), ω_b (bend., a₁), and ω_a (asym. str., b₂), respectively (YZ taken as the molecular plane) and (b) C_s: ω₁ (NO str., a'), ω₂ (NOO bend., a'), and ω₃ (OO str., a'), respectively. Masses of the most abundant isotopes were used: ¹⁴N and ¹⁶O.

^cEnergy respect to NO₂(X²A₁).

B. Location and nature of several surface crossings

At the beginning we considered only the A'/A' intersections because we were mainly interested in the study of the N(⁴S)+O₂(X³Σ_g⁻) reaction. Finally, we took also into account some A'/A'' intersections because they help us to explain some imaginary frequencies appearing in several C_{2v} stationary points, and also for its importance in the study of the N(²D)+O₂(X³Σ_g⁻) reaction.³⁴ The several crossings found among the doublet and quartet A₁, A₂, B₁, and B₂ PES' that could become important for the C_{2v} insertion N(⁴S)+O₂(X³Σ_g⁻) reaction mechanism are summarized in Table V. Figures 1 and 2 show approximately the energy of these crossings. Three crossings between ²B₂ and ²A₁ PES' (I4, I5, and I6) have been located, although the ground ²B₂

PES crosses before with the ²B₁ PES (I9) and latter with the ²A₂ PES. These results agree with previous studies, where information about ²A₁/²B₂ crossings in the C_{2v} region⁴¹ were reported. Another ²B₁/²B₂ crossing was also studied (I10). Two crossings between ⁴B₂ and ⁴A₁ PES' (I1 and I3) were found, and one more that seems to be of the ⁴A₁/⁴A₁ type (I2). The most stable minimum (MIN3) on surface ⁴A₂ crosses twice, one with the ⁴A₁ surface (I7) and another with a ⁴B₂ one (I8).

Regarding to the role of point group symmetry¹⁸ conical intersections can be qualitatively classified as (a) *symmetry required*, when both states are the components of a degenerate irreducible representation (i.e., Jahn–Teller type²²), (b) *symmetry-allowed accidental intersection*, when we have an

TABLE V. Lowest intersections of the A'/A' (I1–I6) and the A'/A'' (I7–I10) types.^a

Intersection ^b	Method	Basis set	R _(NO) /Å	<ONO/°	ΔE/eV ^c
I1(⁴ B ₂ / ⁴ A ₁)	CASSCF(17,12)	aug-cc-pVTZ	1.7654	46.01	6.77
	CASPT2(17,12) G2	"	1.7781	44.62	6.77
I2(⁴ A ₁ / ⁴ A ₁) ^d	CASSCF(17,12)	"	2.0703	54.56	8.28
	CASPT2(17,12) G2	"	"	"	9.10
I3(⁴ A ₁ / ⁴ B ₂)	CASSCF(17,12)	"	1.3739	101.96	4.78
	CASPT2(17,12) G2	"	1.3541	101.69	4.83
I4(² B ₂ / ² A ₁)	CASSCF(17,12)	"	1.7651	46.96	7.15
	CASPT2(17,12) G2	"	1.7648	46.42	7.22
I5(² A ₁ / ² B ₂)	CASSCF(17,12)	"	1.7218	63.69	6.72
	CASPT2(17,12) G2	"	1.6178	62.55	6.77
I6(² B ₂ / ² A ₁)	CASSCF(17,12)	"	1.2617	107.45	1.29
	CASPT2(17,12) G2	"	1.2512	106.53	1.36
	MR-CI ^e	[9s5p1d/5s3p1d]	1.267	107.8	0.96
	MR-CI adiabatic potentials ^f	[9s5p1d/5s3p1d]	1.259	107.4	1.14
I7(⁴ A ₁ / ⁴ A ₂)	CASSCF(13,10) ^g	Huzinaga–Dunning DZ+P	1.274	107.4	1.14
	experimental ^h	"	1.246	103.1	1.21
	CASSCF(17,12)	aug-cc-pVTZ	1.3665	88.96	4.46
I8(⁴ A ₂ / ⁴ B ₂)	CASPT2(17,12) G2	"	1.3807	90.73	4.42
	CASSCF(17,12)	"	1.3053	144.31	4.55
I9(² B ₂ / ² B ₁)	CASPT2(17,12) G2	"	1.3061	142.02	4.34
	CASSCF(17,12)	"	1.8598	41.70	6.09
I10(² B ₁ / ² B ₂)	CASPT2(17,12) G2	"	1.8470	41.87	6.42
	CASSCF(17,12)	"	1.3591	74.75	3.40
	CASPT2(17,12) G2	"	1.3490	74.33	3.59

^aThe CASPT2 G2 energies and geometries reported were derived from a grid of points by using bicubic splines (Ref. 31).

^bThe A/B notation indicates an intersection of surface A (lower energy on the left) with surface B (lower energy on the right) according to Figs. 1 and 2.

^cEnergy with respect to NO₂(X²A₁).

^dFor the I2 intersection only the CASPT2 energy at the CASSCF geometry is given.

^eReference 3.

^fReference 4.

^gReference 12.

^hReferences 6, 7, and 8.

intersection of two states of different spatial symmetry, and (c) *same-symmetry accidental intersections* between states of the same symmetry. All the intersections we have found are symmetry-allowed accidental intersections, with the exception of I2, which is a same-symmetry accidental intersection. In the present work, this approximate classification has been applied by using the C_{2v} highest molecule group symmetry, due to the fact that this classification could depend whether C_{2v} or C_s symmetry are considered.⁴²

To locate the intersections we have computed a grid of points for each surface using the Jacobi coordinates shown in Fig. 1 (r and R) at the CASSCF and CASPT2 G2 levels. The range of R goes from 0.0 to 4.5 Å and for r it goes from 1.0 to 2.5 Å. We have used an increment of 0.1 Å except for the reactants asymptotic region ($R > 2.5$ Å) where it is longer and increases as R increases. Doing the energy difference between different diabatic surfaces we were able to extract, approximately, the intersection seam for each case. To have an intersection between two adiabatic states two conditions have to be satisfied. If we express the two adiabatic states (1 and 2) as a combination of two diabatic states (A and B) and we solve the 2×2 Hamiltonian problem between these diabatic states, we will see that to have a crossing (i.e., $E_1 = E_2$, E_1 , and E_2 being the energies of the two adiabatic states) the two conditions to be fulfilled are $H_{AA}(\mathbf{q}) = H_{BB}(\mathbf{q})$ and $H_{AB}(\mathbf{q}) = 0$. Therefore, the dimension of the intersection space will be $(N-2)$ when both states are of the same spatial symmetry and $(N-1)$ when both are of different spatial symmetry, because the $H_{AB}(\mathbf{q}) = 0$ condition will be satisfied by symmetry in this last case (N being the number of internal degrees of freedom of the system). Hence, the symmetry of the system has to be taken into account too. If we are working in a higher symmetry group (i.e., C_{2v} instead of C_s) we have less internal degrees of freedom to satisfy both conditions (M instead of N , with $M < N$). For the first type of intersections (i.e., A'/A') the dimension of the intersection space corresponds to a line for C_{2v} ($M-1=1$) and C_s ($N-2=1$) geometries when both surfaces belong to a different irreducible representation in C_{2v} , but to the same one in C_s ; the dimension of this space is a point for C_{2v} ($M-2=0$) geometries and a line for C_s ($N-2=1$) geometries if both surfaces are of the same symmetry in C_{2v} and in C_s symmetries. In surface intersections, where the dimension of the intersection space be lower at C_{2v} geometries than at C_s ones, the intersection space will be probably part of a C_s symmetry intersection that passes through C_{2v} .

Intersections I1, I3, I4, I5, and I6 correspond to the first case and I2 to the second one (Table V). On the other hand, if the crossing implies two surfaces of different symmetry in C_{2v} and in C_s (i.e., the A'/A'' type), the dimension of the intersection space is a line in C_{2v} ($M-1=1$) but a plane in C_s ($N-1=2$), as occurs in I7, I8, I9, and I10.

Once we had found the C_{2v} seams, we have chosen a local grid around these intersection seams between the diabatic surfaces and we have fit these points for each surface involved in the crossing by means of bicubic splines, obtaining a root mean square deviation less than 1 kcal/mol in all cases. With the local fit we have interpolated more points for each surface and doing the energy difference we have ob-

tained the intersection seam again in a more accurate way. The minimum energy point on each seam corresponds to the given geometries reported in Table V.

Intersection I2 has been located in a different way because it takes place between two states of the same spatial symmetry (4A_1). It corresponds to a point in C_{2v} instead of a line as in the other cases. Both 4A_1 PES' (i.e., the ground one and the first excited one) were calculated using the two-state-averaged methodology.²⁶ The intersection point has been located as the minimum point in the energetic difference hypersurface $\Delta E = E(2{}^4A_1) - E(1{}^4A_1)$. I2 was located at $R_{\text{NO}} = 2.0703$ Å and $\angle \text{ONO} = 54.56^\circ$, with $\Delta E = 0.07$ kcal/mol at the CASSCF level. We had not located I2 at the CASPT2 level due to problems with some points near the intersection because both roots were interchanged, which means that the ground state was more unstable than the excited one in those points. Because of that we were not able to see a minimum point in the ΔE hypersurface at the CASPT2 level. This problem could be solved using the multistate CASPT2 method,⁴³ but this intersection is so far from the MEP for the $\text{N}({}^4S) + \text{O}_2$ ($X^3\Sigma_g^-$) reaction and therefore we were not interested in its location in so extensive a way.

To verify much more our results about the intersections we have tried to locate as well some of those with GAUSSIAN 98 program,^{32,44} by using the CASSCF method with a reduced active space (7,6) and a Pople basis set [6-31G(d)] to decrease the effort of the calculation. We were able to find two intersections, I6 and I10, which agree with our results. For I6 and I10 we have found CASSCF C_s geometries with $R_{\text{NO}} = 1.1982$ and 1.3868 Å and $\angle \text{ONO} = 109.85^\circ$, and $R_{\text{NO}} = 1.3342$ and 1.3563 Å and $\angle \text{ONO} = 78.90^\circ$, respectively, to be compared with the similar but C_{2v} structures indicated in Table V. At this *ab initio* level the energy differences between the two states involved in the crossing were the following: 0.04 kcal/mol for I6 and 0.06 kcal/mol for I10. The slightly difference for I6 in R_{NO} distance can be explained in terms of the different active space and basis set used, but as it is shown in Table V the C_{2v} structure agrees with previous theoretical^{3,4,12} and experimental⁶⁻⁸ results found in the literature. For I6 we have also computed the energy difference between both states implicated in the crossing and we have obtained a value of 8×10^{-3} kcal/mol at CASSCF(17,12)/aug-cc-pVTZ level, which confirms that we have found the true geometry to describe the intersection.

The bending of NO_2 structures has been previously studied,^{9,10} where intersections between doublet and quartet states have been predicted, but not located. The approximate angles at what intersections take place in those papers are close to our results. The possible connections between the NO_2 minima and the $\text{N} + \text{O}_2$ reactants has not been studied up to now. Previous studies only explored the bending region between 70° – 180° , but did not study smaller angles that would correspond to I1, I2, I4, I5, and I9 intersections.

We have studied the orbitals responsible for the electronic configuration exchange in each crossing (Table VI). For I1 the configurations for the lower state before and after the crossing change one electron between $7a_1$ and $5b_2$ orbitals, both are NO antibonding, but the former is OO bond-

TABLE VI. Electronic configuration exchange for each intersection.^a

Intersection	Electronic configurations ^b	c_i^{2c}
I1 (⁴ B ₂ / ⁴ A ₁)	(6a ₁) ² (7a ₁) ¹ (1b ₁) ² (2b ₁) ¹ (1a ₂) ¹ (2b ₂) ² (3b ₂) ² (4b ₂) ⁰ (5b ₂) ⁰	76%
	(6a ₁) ² (7a ₁) ⁰ (1b ₁) ² (2b ₁) ¹ (1a ₂) ¹ (2b ₂) ² (3b ₂) ² (4b ₂) ⁰ (5b ₂) ¹	85%
I2 (⁴ A ₁ / ⁴ A ₁)	(6a ₁) ² (7a ₁) ⁰ (1b ₁) ² (2b ₁) ¹ (1a ₂) ¹ (2b ₂) ² (3b ₂) ² (4b ₂) ⁰ (5b ₂) ¹	76%
	(6a ₁) ² (7a ₁) ⁰ (1b ₁) ² (2b ₁) ¹ (1a ₂) ¹ (2b ₂) ² (3b ₂) ² (4b ₂) ¹ (5b ₂) ⁰	78%
I3 (⁴ A ₁ / ⁴ B ₂)	(6a ₁) ² (7a ₁) ⁰ (1b ₁) ² (2b ₁) ¹ (1a ₂) ¹ (2b ₂) ² (3b ₂) ² (4b ₂) ¹ (5b ₂) ⁰	85%
	(6a ₁) ¹ (7a ₁) ⁰ (1b ₁) ² (2b ₁) ¹ (1a ₂) ¹ (2b ₂) ² (3b ₂) ² (4b ₂) ² (5b ₂) ⁰	88%
I4 (² B ₂ / ² A ₁)	(6a ₁) ² (7a ₁) ¹ (1b ₁) ² (2b ₁) ¹ (1a ₂) ¹ (2b ₂) ² (3b ₂) ² (4b ₂) ⁰ (5b ₂) ⁰	74%
	(6a ₁) ² (7a ₁) ⁰ (1b ₁) ² (2b ₁) ¹ (1a ₂) ¹ (2b ₂) ² (3b ₂) ² (4b ₂) ¹ (5b ₂) ⁰	68%
I5 (² A ₁ / ² B ₂)	(6a ₁) ² (7a ₁) ⁰ (1b ₁) ² (2b ₁) ¹ (1a ₂) ¹ (2b ₂) ² (3b ₂) ² (4b ₂) ¹ (5b ₂) ⁰	44%
	(6a ₁) ² (7a ₁) ⁰ (1b ₁) ² (2b ₁) ⁰ (1a ₂) ² (2b ₂) ² (3b ₂) ² (4b ₂) ¹ (5b ₂) ⁰	61%
I6 (² B ₂ / ² A ₁)	(6a ₁) ² (7a ₁) ⁰ (1b ₁) ² (2b ₁) ⁰ (1a ₂) ² (2b ₂) ² (3b ₂) ² (4b ₂) ¹ (5b ₂) ⁰	85%
	(6a ₁) ¹ (7a ₁) ⁰ (1b ₁) ² (2b ₁) ⁰ (1a ₂) ² (2b ₂) ² (3b ₂) ² (4b ₂) ² (5b ₂) ⁰	89%
I7 (⁴ A ₁ / ⁴ A ₂)	(6a ₁) ² (7a ₁) ⁰ (1b ₁) ² (2b ₁) ¹ (1a ₂) ¹ (2b ₂) ² (3b ₂) ² (4b ₂) ¹ (5b ₂) ⁰	85%
	(6a ₁) ¹ (7a ₁) ⁰ (1b ₁) ² (2b ₁) ¹ (1a ₂) ² (2b ₂) ² (3b ₂) ² (4b ₂) ¹ (5b ₂) ⁰	91%
I8 (⁴ A ₂ / ⁴ B ₂)	(6a ₁) ¹ (7a ₁) ⁰ (1b ₁) ² (2b ₁) ¹ (1a ₂) ² (2b ₂) ² (3b ₂) ² (4b ₂) ¹ (5b ₂) ⁰	91%
	(6a ₁) ¹ (7a ₁) ⁰ (1b ₁) ² (2b ₁) ¹ (1a ₂) ¹ (2b ₂) ² (3b ₂) ² (4b ₂) ² (5b ₂) ⁰	88%
I9 (² B ₂ / ² B ₁)	(6a ₁) ² (7a ₁) ¹ (1b ₁) ² (2b ₁) ¹ (1a ₂) ¹ (2b ₂) ² (3b ₂) ² (4b ₂) ⁰ (5b ₂) ⁰	77%
	(6a ₁) ² (7a ₁) ⁰ (1b ₁) ² (2b ₁) ¹ (1a ₂) ² (2b ₂) ² (3b ₂) ² (4b ₂) ⁰ (5b ₂) ⁰	72%
I10 (² B ₁ / ² B ₂)	(6a ₁) ² (7a ₁) ⁰ (1b ₁) ² (2b ₁) ¹ (1a ₂) ² (2b ₂) ² (3b ₂) ² (4b ₂) ⁰ (5b ₂) ⁰	88%
	(6a ₁) ² (7b ₁) ⁰ (1b ₁) ² (2b ₁) ⁰ (1a ₂) ² (2b ₂) ² (3b ₂) ² (4b ₂) ¹ (5b ₂) ⁰	85%

^aFor each A/B intersection, the first electronic configuration corresponds to the A state and the second one to the B state.

^bThe inner orbitals present the same occupation in all cases [i.e., (3a₁)²(4a₁)²(5a₁)²] and they are not shown.

^cThe weight of the most important CSF in the CASSCF(17,12) wave function for this region of the PES.

ing and the later OO antibonding. The inclusion of one electron in an antibonding OO orbital (5b₂) favors the breaking of the OO distance that is necessary to insert the N atom. For I2, one electron initially in the 5b₂ orbital goes to the 4b₂ one without changing the electronic state symmetry (⁴A₁). Both orbitals are OO antibonding but the 4b₂ is NO bonding and its occupation favors the NO bond formation in the insertion path. In I3, the 6a₁ orbital loses an electron that goes to the 4b₂ orbital, the former is OO bonding and the latter OO antibonding, becoming more stable as the insertion reaction goes forward.

Intersections of ⁴A'/⁴A'' type show the same behavior (Table VI). In I7 we have an electron that goes from the 6a₁ orbital (OO bonding) to the 1a₂ one (OO antibonding) favoring the OO breaking. In I8 one of the 1a₂ electrons goes to the 4b₂ orbital, both are OO antibonding orbitals, but in the 4b₂ appears a bonding NO interaction that makes possible the NO bond formation. For the doublet case we have the same type of explanation for the electronic configuration exchange. In I4 an electron in the 7a₁ orbital goes to the 4b₂ orbital, both are NO antibonding, but only the latter is OO antibonding. In I5, the 2b₁ electron jumps to the 1a₂ orbital, the former does not favor the NO bond formation, and the OO bond breaking because it is NO antibonding and OO bonding, but the a₂ is NO no bonding and OO antibonding and favors the insertion mechanism with the necessary OO breaking and NO formation. For I6, the occupation changes between the 6a₁ orbital and the 4b₂ one, where the OO interaction becomes antibonding and the NO no bonding favoring the insertion of a N atom as in the I5 case above. For the second type of intersections (²A'/²A'') the change is as follows: for I9 one 7a₁ electron jumps to the 1a₂ orbital more stable after intersection due to an antibonding OO in-

teraction, which becomes less repulsive as the OO distance increases in the insertion path. In I10, the 2b₁ electron goes to the 4b₂ orbital; the latter becomes more stable after intersection for the same reason that the 1a₂ orbital above in the I9 case.

To sum up, different interactions are important in the C_{2v}-insertion mechanism depending on the surface region we are exploring. At the beginning of the insertion path the main ones are the NO antibonding interaction and the OO bonding one (i.e., a N atom and an O₂ molecule separately). In the barrier region the OO antibonding interaction becomes important and sometimes the NO no bonding one too (i.e., breaking the OO bond to insert the N atom). At the insertion end the main interaction is the NO bonding one (i.e., the OO bond is broken and the NO bond is formed).

C. Topological analysis of the surface crossings

To study the topology of the potential energy surfaces around the intersections, two vectors can be defined, the gradient difference (\mathbf{x}_1) and the gradient of the interstate coupling (\mathbf{x}_2) vectors:^{44,45}

$$\mathbf{x}_1 = \frac{\partial(E_1 - E_2)}{\partial \mathbf{q}}, \quad (2)$$

$$\mathbf{x}_2 = \left\langle \mathbf{C}_1 \left(\frac{\partial \mathbf{H}}{\partial \mathbf{q}} \right) \mathbf{C}_2 \right\rangle, \quad (3)$$

where \mathbf{C}_1 and \mathbf{C}_2 are the configuration interaction eigenvectors and \mathbf{H} is the corresponding CI or MC-SCF Hamiltonian. The vector \mathbf{x}_2 is parallel to the nonadiabatic coupling.⁴⁵ In general, if there are N internal coordinates, N-2 coordinates

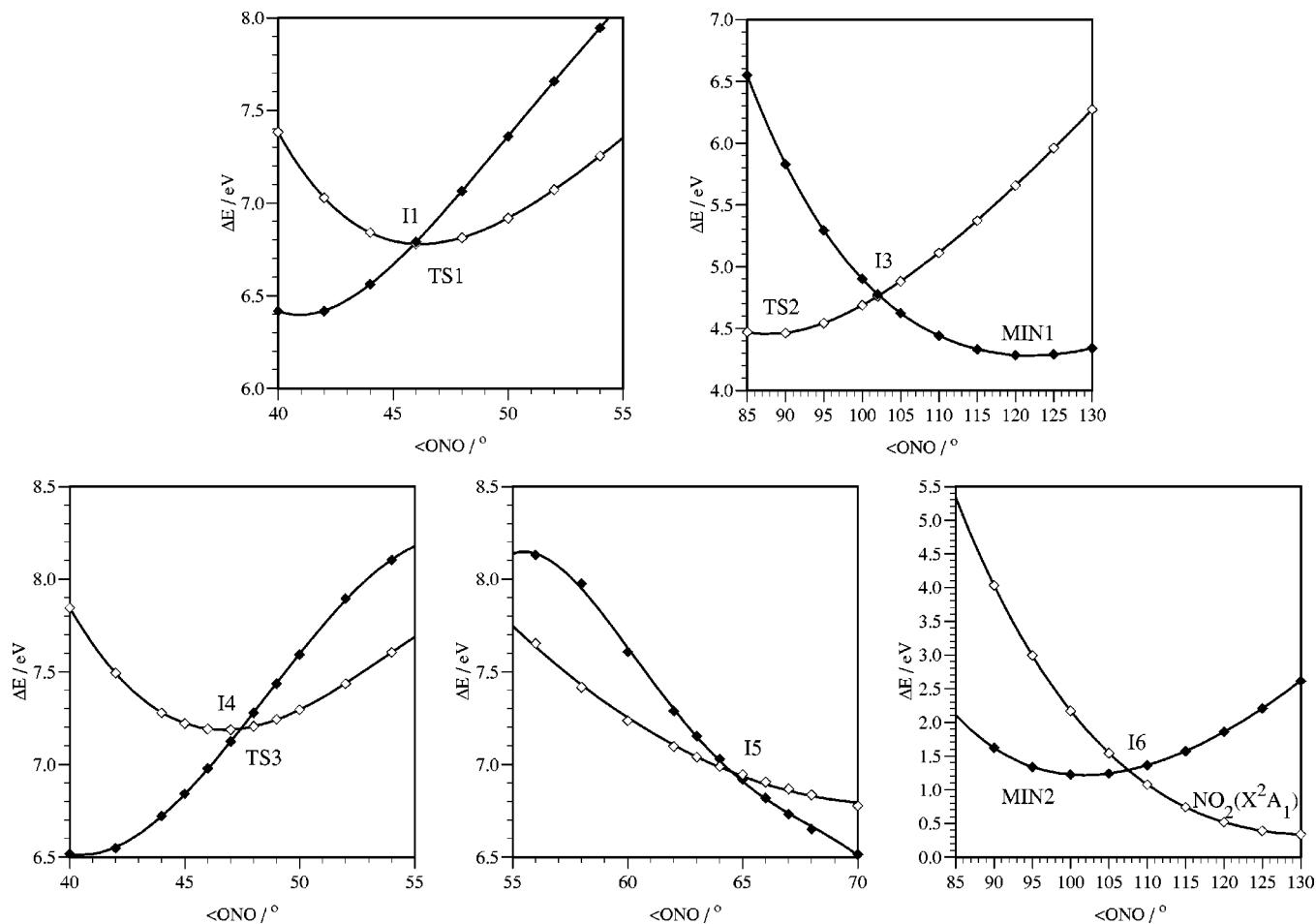


FIG. 3. Bending diagrams at the CASSCF(17,12)/aug-cc-pVTZ level for different A_1/B_2 intersections. (\blacklozenge) represents the B_2 state and (\diamond) the A_1 one. The calculations were performed in C_{2v} symmetry with the NO distance kept frozen at the corresponding value reported in Table V for each intersection. Zero of energy in the $\text{NO}_2(X^2A_1)$ molecule.

will form the *intersection space*, where both adiabatic states are degenerated, and the other two coordinates (\mathbf{x}_1 and \mathbf{x}_2) will form the *branching space*, where both adiabatic states lose their degeneracy.

We have studied the topology of the intersections between states of the same symmetry in C_s (i.e., A'/A') but not those of different symmetry in C_s (i.e., A'/A''). This fact was essentially motivated because the second type of intersections cannot be conical nor were involved in the title reaction. This only occurs in triatomic molecules that have all vibrational modes symmetric (a') because they do not have a no totally symmetric mode (as b_2 in C_{2v}) that can couple the degenerate states.¹⁸ The topology of intersection I2 has not been studied either because, as we previously see, it is located so far from the minimum energy path.

In our case we have represented the energies in front of the $\angle\text{ONO}$ angle and respect to a coordinate, which breaks the C_{2v} symmetry of the system (i.e., x). This latter coordinate is defined as $x = (R_{(\text{NO})} + n\Delta R) - (R_{(\text{NO})} - n\Delta R) = 2n\Delta R$, where $n = 1, 2, 3, 4, \dots$, is the point number, $\Delta R = 0.01 \text{ \AA}$ and $R_{(\text{NO})}$ is the NO distance given in Table V for each intersection. We have used the above-mentioned coordinates after identifying the vectors of the branching space by using the GAUSSIAN 98 code,³² the x_1 vector corresponds

basically to the bending motion (a_1 symmetry), and the x_2 vector to the asymmetric NO stretching (b_2 symmetry) of the C_{2v} structure, with minor participation of the bending motion. In order to compute the bending motion for I1, I3, I4, I5, and I6 at the CASSCF level, the NO distances were kept fixed at their corresponding intersection values (Table VI) and the ONO angle was varied in the appropriate range for each case (Fig. 3). Intersections I1 and I4 take place at small angles (around 46°), which correspond to the beginning of the insertion path. I5 is located at about 64° , and I3 and I6 appear at the end of the insertion path, when the C_{2v} minima have been formed, at around 105° .

Intersections can be classified regarding their local topology,²³ which affects the probability to have a radiationless decay of an excited state. An intersection can be classified as *peaked* when it has the form of a tilted double cone, where the lower adiabatic surface decreases in all directions from the intersection point and the upper adiabatic surface increases in all directions from the same point. Another pattern is the *sloped* one, where both surfaces have downhill slopes and touch each other at the crossing points in the branching space. An *intermediate* pattern can be possible where there exists a line along which E_1 has a zero slope on

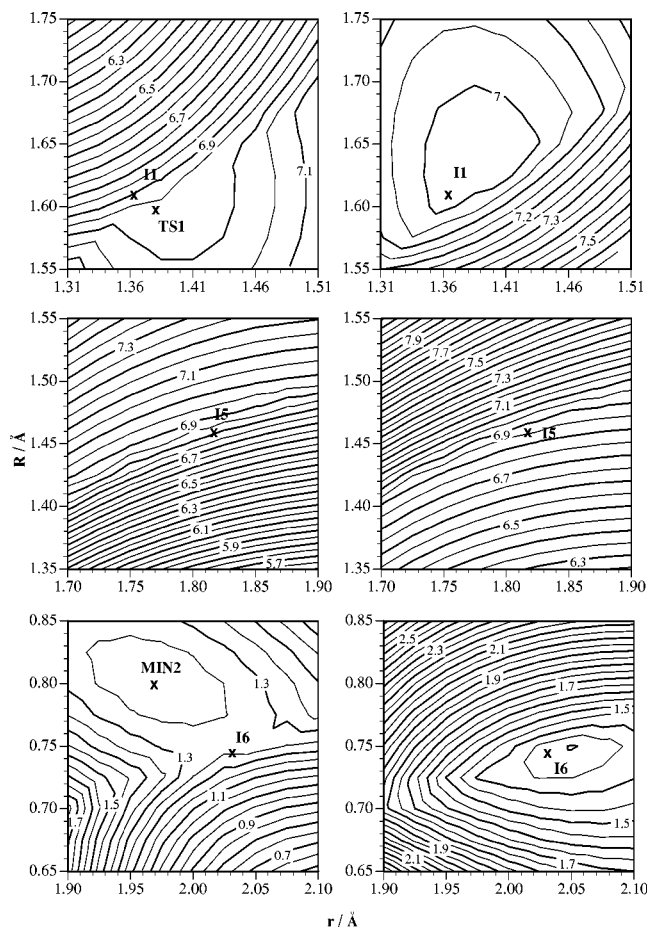


FIG. 4. Contour diagrams around I1 (intermediate), I5 (sloped), and I6 (peaked) in the Jacobi space (r and R) at the CASSCF(17,12)/aug-cc-pVTZ level. The lower adiabatic PES for each intersection is depicted on the left, and the upper adiabatic one on the right. The contour interval is 0.05 eV. Zero of energy in the NO₂ (X^2A_1) molecule. Crosses show the location of the lowest point in each intersection and also other stationary points.

one side of the intersection and E_2 has zero slope on the other side of the intersection. We have found these three types of topologies: (a) peaked intersections: I3 and I6; (b) sloped intersections: I5; and (c) *intermediate* intersections: I1 and I4. The last case implies intersections that almost coincide with stationary points (null slope by definition). Thus, I1 is very close to TS1 and I4 to TS3.

In Fig. 4 the ground adiabatic surface and the first excited one are shown for three representative intersections: I1 (intermediate), I5 (sloped), and I6 (peaked) using Jacobi coordinates (i.e., r and R) at the CASSCF(17,12)/aug-cc-pVTZ level; the same topological results were found at the CASPT2 level too. For the intermediate case (I1), apart from the change in the slope, TS1 appears very close to the intersection seam. In I5 only, it is possible to see the change of slope in both adiabatic surfaces. In the I6 plot, the lower surface shows a saddle point and a minimum (MIN2) very close to the intersection point. The excited surface presents another minimum. In the approximate plot shown in Fig. 2 for this crossing at the CASPT2 G2/aug-cc-pVTZ level, the MIN2 seems to be in the excited PES but really it is in the lower surface as in the CASSCF results.

We have drawn in Fig. 5 an estimated asymmetric stretch around the I1–I6 intersections at the CASSCF(17,12)/aug-cc-pVTZ level. To do this, we have increased one NO distance 0.01 Å and have decreased another one of the same quantity. The ONO angle has been frozen to its intersection value reported in Table V. In all cases we see how both surfaces separate each other from $x=0$. For I6 we can see a pseudo-Jahn–Teller distortion with an asymmetric minimum (NO distances equal 1.2117 and 1.3117 Å) around 1.3 kcal/mol below the conical intersection. For I5 and I4 an opposite behavior is found, and two asymmetric maxima for the excited surfaces are observed (NO distances equal to 1.6951 and 1.8351 Å, and 1.6918 and 1.7518 Å for I4 and I5, respectively). In all cases the excited surface is funneled into the intersection region ($x=0$), where there is a minimum. On the other hand, the ground surface has a maximum at the intersection and thereby the minimum energy path in the ground surface has the tendency to avoid the intersection point and to take place through asymmetric geometries (i.e., C_s symmetries). This explains the problems to locate the transition states for the C_{2v} -insertion mechanism through the doublet and quartet PES', where the strictly C_{2v} stationary points found are second-order saddle points (TS5' and TS4', as given in Table IV), being preferred a direct C_s -insertion mechanism for both PES' (TS5 and TS4 for the $^2A'$ and $^4A'$ PES', respectively, as shown in Table IV).

We have also calculated the splitting between both adiabatic surfaces at the crossing point of the two diabatic surfaces (geometries given in Table V) by means of *ab initio* C_s calculations. The following values have been obtained at the CASSCF(17,12)/aug-cc-pVTZ level: 1.76 kcal/mol (I1), 0.45 kcal/mol (I3), 3.60 kcal/mol (I4), 0.45 kcal/mol (I5), and 8×10^{-3} kcal/mol (I6). As can be seen, the energy values obtained for the intermediate intersections (I1) and (I4) are very high, possibly because the search method was not accurate enough for these intersections. The other intersections showed much lower values (under 0.5 kcal/mol). We have also observed that the point of closest approach between both adiabatic surfaces is not exactly at the same position as that of the crossing between both diabatic surfaces, the former being slightly shifted from the MEP.

Figure 6 shows contours around I6 for its approximate branching space (i.e., x , \angle ONO), which allows now (not seen in Fig. 4 due to the C_{2v} symmetry) to see directly the mentioned transition state (TS6) that connects MIN2 with the NO₂(X^2A_1) molecule through C_s symmetry. Due the symmetry of the system there are two equivalent transition states. The problem mentioned in Sec. III A that respects the dispersion of the theoretical asymmetric frequencies of MIN2 (Table I), which are quite different from the experimental value, can be now better rationalized. The proximity of I6 implies an asymmetric NO₂ distortion along the minimum energy path that affects the MIN2 asymmetric stretching frequency. The low value obtained for this frequency can be understood, considering the bifurcation nature of the surface between MIN2 and I6. The nature of this reaction path from the MIN2 (2B_2) to the NO₂(X^2A_1) molecule on the lowest $^2A'$ surface has been previously discussed.⁴⁶ In that paper an asymmetric path was also de-

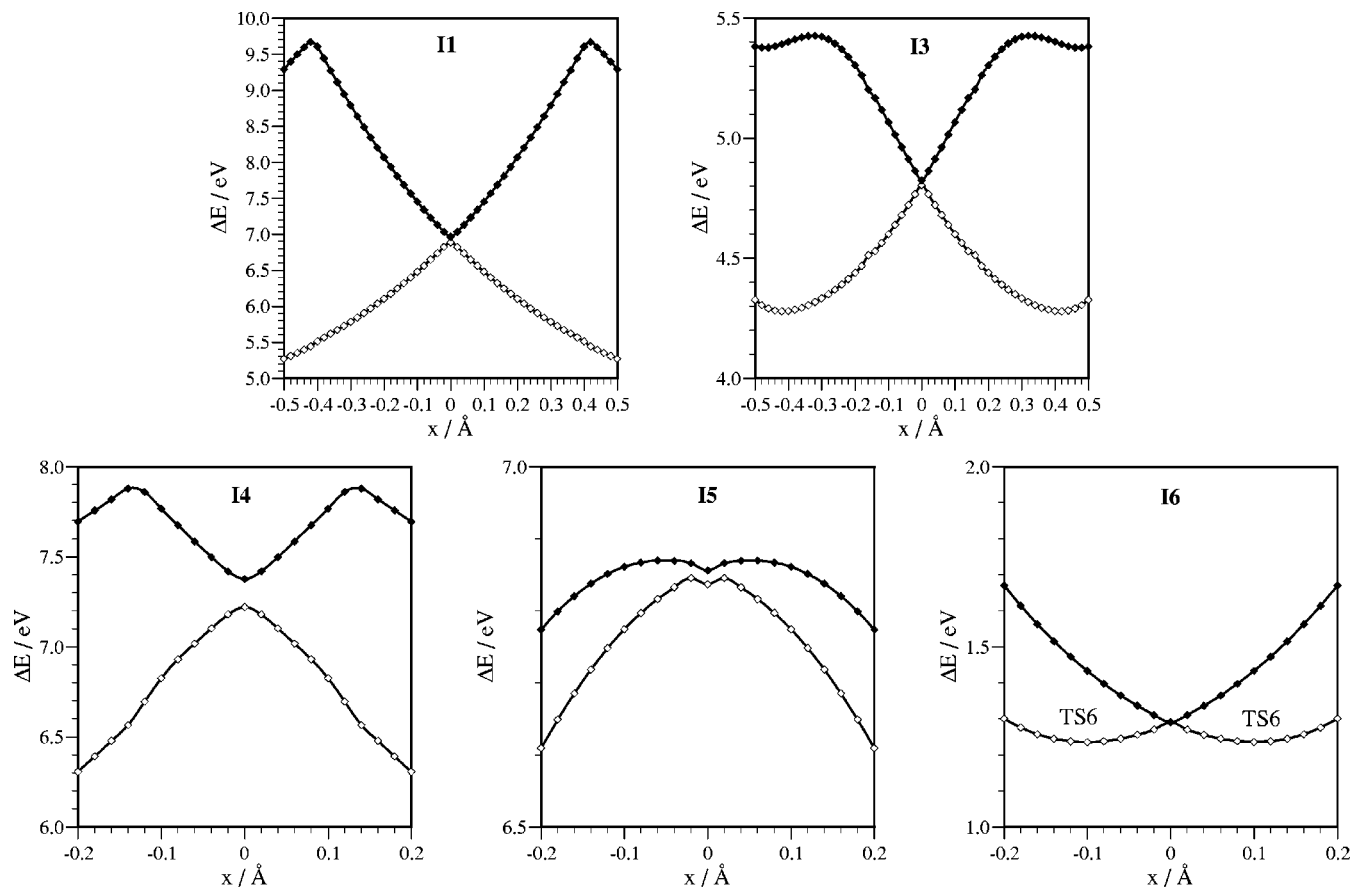


FIG. 5. Asymmetric distortion (x) at the CASSCF(17,12)/aug-cc-pVTZ level for different A_1/B_2 intersections. The x coordinate is defined as $x = (R_{(\text{NO})} + n \Delta R) - (R_{(\text{NO})} - n \Delta R) = 2n \Delta R$, where $n = 1, 2, 3, 4, \dots$, is the point number, $\Delta R = 0.01 \text{ \AA}$ and $R_{(\text{NO})}$ is the NO distance given in Table V for each intersection. Negative values are obtained by NO interchange symmetry. The $\angle \text{ONO}$ angle was kept frozen at the value corresponding at each intersection (Table V). (\diamond) represents the ground A' adiabatic curve and (\blacklozenge) the first excited A' adiabatic one. Zero of energy in the $\text{NO}_2 (X^2A_1)$ molecule.

scribed, and MIN2 was characterized as a saddle point because its asymmetric stretching initialized the through down to the $\text{NO}_2 (X^2A_1)$ minimum. We think this bifurcation point due to the asymmetric motion begins in a region between MIN2 and I6 (i.e., TS6), but not exactly in MIN2, because we have obtained a real frequency for the asymmetric

stretching at this point. In Fig. 6 we can see that the intersection I6 (Table V) and TS6 [$R_{(\text{NO})} = 1.2117, 1.3117 \text{ \AA}$, $\angle \text{ONO} = 107.5^\circ$, $\Delta E = 1.23 \text{ eV}$ at the CASSCF (17,12)/aug-cc-pVTZ level, or 1.30 eV at the CASPT2 level] are so close that also a nonadiabatic recrossing could be important between both surfaces.¹⁸

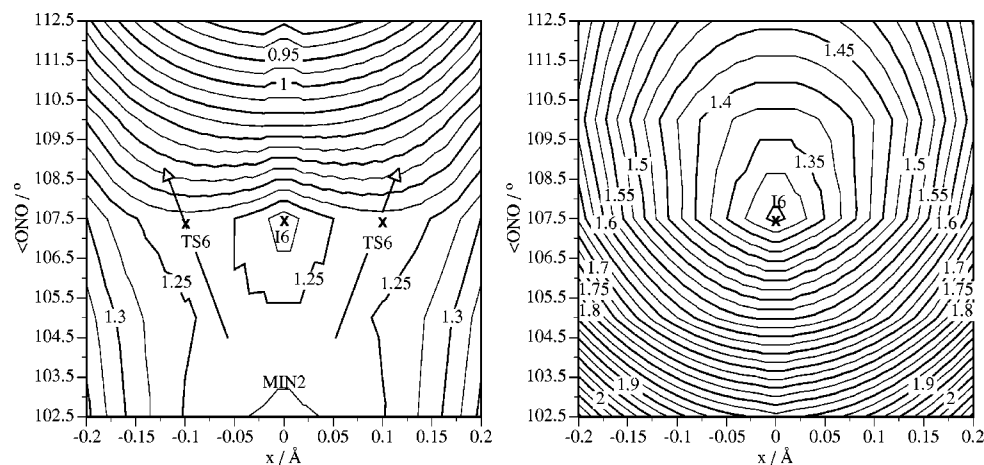


FIG. 6. Contour diagrams around I6 with respect to the x and $\angle \text{ONO}$ coordinates at the CASSCF(17,12)/aug-cc-pVTZ level. The lower adiabatic PES of this intersection is depicted on the left, and the upper adiabatic one on the right. The contour interval is 0.025 eV . Zero of energy in the $\text{NO}_2 (X^2A_1)$ molecule. Crosses show the location of the intersection I6 and the TS6.

IV. CONCLUSIONS AND REMARKS

This work presents a theoretical study of the lowest doublet and quartet potential energy surfaces involved in the C_{2v} -insertion mechanism of the $N(^4S) + O_2(X^3\Sigma_g^-) \rightarrow NO(X^2\Pi) + O(^3P)$ reaction. *Ab initio* molecular electronic structure CASSCF and CASPT2 methods with a standard correlation-consistent Dunning's basis sets (aug-cc-pVTZ) and a full-valence active space were used to characterize the stationary points and the different conical intersections for the A_1 , B_1 , A_2 , and B_2 doublet and quartet PES'. The UB3LYP DFT method was also used to facilitate the search of the stationary points and to make IRCs for the transition states, producing similar results to the *ab initio* ones. Thus, several minima, transition states, and surface crossings have been found along the different C_{2v} -MEPs connecting reactants and products on these surfaces. The results agree very well with available experimental data [i.e., for $NO_2(^2A_1)$, $MIN2(^2B_2)$, $NO_2(^2\Pi_u)$] and with other previous *ab initio* calculations.

Six A'/A' and four A'/A'' -type surface crossings were located and classified by their topology on the mentioned doublet and quartet PES'. Among these, only one (i.e., $^2B_2/^2A_1$) had been reported previously in theoretical and experimental studies. The results presented here are almost coincident with them and can be taken as a validation of the theoretical method used. Although these surface crossings produce important changes (i.e., changes of slope, maxima, cusps,...) in the shape of the adiabatic surfaces ($^2A'$ and $^4A'$) in its C_{2v} geometrical region, their influence on the $N(^4S) + O_2(X^3\Sigma_g^-)$ reaction should be small at low collision energies apart from possible geometric phase effects. Major importance could be expected for the reaction with electronically excited reactants [i.e., $N(^4S) + O_2(a^1\Delta_g)$ or $N(^2D) + O_2(X^3\Sigma_g^-)$], where this region of the PES is much more energetically accessible and possible nonadiabatic decays to the ground PES' could be likely throughout the reaction.

There was demonstrated that the direct C_{2v} -insertion mechanism studied here presented very high-energy barriers (3.11 and 2.54 eV for the lowest doublet and quartet PES' at the CASPT2 G2/aug-cc-pVTZ level, respectively), clearly being more unfavorable than the direct C_s -abstraction or indirect C_s -insertion mechanisms reported in Paper I for the same reaction, which showed 0.20 and 0.55 eV energy barriers (C_s -abstraction mechanism), respectively, at the same *ab initio* level. Moreover, the corresponding C_{2v} -symmetry transition states [TS4'($^4A'$) and TS5'($^2A'$)] were located as second-order saddle points, giving place under an asymmetric distortion to true C_s transition states [TS4($^4A'$) and TS5($^2A'$)] with lower-although still high-energy barriers (2.13 and 2.54 eV values, respectively), in comparison to the other competitive microscopic mechanisms.

The present results complete the *ab initio* study initiated in Paper I aiming to describe the full topology (i.e., C_s and C_{2v} geometries) of the lowest adiabatic doublet and quartet PES' involved in the title reaction. All the theoretical information obtained about the stationary points and the different surface crossings along with new grids of *ab initio* points has been used in the construction of two analytical PES' ($^2A'$

and $^4A'$)⁴⁷ that will improve the quality of previous analytical ones. A dynamics and kinetics study on both PES' is in progress at present in our research group to see the importance of the several microscopic mechanisms found for this reaction and to reveal the influence of some of the conical intersections found for this system.

ACKNOWLEDGMENTS

This work has been supported by the "Dirección General de Enseñanza Superior (Programa Sectorial de Promoción General del Conocimiento)" of the Spanish Ministry of Education and Culture (DGES Project Ref. PB 98-1209-C02-01). Financial support from the European Union (INTAS Project Ref. 99-00701) and the "Generalitat" (Autonomous Government) of Catalonia (Projects Refs. 1998SGR 0008 and 2000SGR 00016) is also acknowledged. C.O. thanks the Spanish Ministry of Education and Culture for a predoctoral research grant. The authors are grateful to the "Center de Computació i Comunicacions de Catalunya (C⁴-CESCA/CEPBA)" for providing a part of the computer time.

- ¹R. Sayós, C. Oliva, and M. González, *J. Chem. Phys.* **115**, 1287 (2001).
- ²M. W. Chase, Jr., C. A. Davies, J. R. Downey, Jr., D. J. Frurip, R. A. McDonald, and A. N. Syverud, *J. Phys. Chem. Ref. Data* **14**, 1 (1985).
- ³G. Hirsch and R. J. Buenker, *Can. J. Chem.* **63**, 1542 (1985).
- ⁴G. Hirsch, R. J. Buenker, and C. Petrongolo, *Mol. Phys.* **73**, 1085 (1991).
- ⁵E. Leonardi, C. Petrongolo, G. Hirsch, and R. J. Buenker, *J. Chem. Phys.* **105**, 9051 (1996).
- ⁶J. C. D. Brand, K. J. Cross, and A. R. Hoy, *Can. J. Phys.* **57**, 428 (1979).
- ⁷A. J. Merer and K.-E. J. Hallin, *Can. J. Phys.* **56**, 838 (1978).
- ⁸M. Krauss, R. J. Celotta, S. R. Mielczarek, and C. E. Kuyatt, *Chem. Phys. Lett.* **27**, 285 (1974).
- ⁹G. D. Gillispie and A. U. Khan, *J. Chem. Phys.* **63**, 3425 (1975).
- ¹⁰C. F. Jackels and E. R. Davidson, *J. Chem. Phys.* **65**, 2941 (1976).
- ¹¹Y. Xie, R. D. Davy, B. F. Yates, C. P. Blahous III, Y. Yamaguchi, and H. F. Schaefer III, *Chem. Phys.* **135**, 179 (1989).
- ¹²C. P. Blahous, B. F. Yates, Y. Xie, and H. F. Schaefer III, *J. Chem. Phys.* **93**, 8105 (1990).
- ¹³U. Kaldor, *Chem. Phys. Lett.* **185**, 131 (1991).
- ¹⁴C. Meredith, R. D. Davy, G. E. Quelch, and H. F. Schaefer III, *J. Chem. Phys.* **94**, 1317 (1991).
- ¹⁵H. Kato and M. Baba, *Chem. Rev.* **95**, 2311 (1995).
- ¹⁶D. R. Yarkony, *Rev. Mod. Phys.* **68**, 985 (1996).
- ¹⁷P. W. Kash, G. C. G. Waschewsky, R. E. Morss, L. J. Butler, and M. M. Francl, *J. Chem. Phys.* **100**, 3463 (1994).
- ¹⁸D. R. Yarkony, *Acc. Chem. Res.* **31**, 511 (1998).
- ¹⁹G. Herzberg and H. C. Longuet-Higgins, *Discuss. Faraday Soc.* **35**, 77 (1963); C. A. Mead and D. G. Truhlar, *J. Chem. Phys.* **70**, 2284 (1979).
- ²⁰Y.-S. M. Wu, A. Kuppermann, and B. Lepetit, *Chem. Phys. Lett.* **186**, 319 (1991). Y.-S. M. Wu and A. Kuppermann, *ibid.* **201**, 178 (1993); Y.-S. M. Wu and A. Kuppermann, *ibid.* **235**, 105 (1995).
- ²¹S. Xantheas, S. T. Elbert, and K. Ruedenberg, *J. Chem. Phys.* **93**, 7519 (1990).
- ²²T. A. Barckholtz and T. A. Miller, *J. Phys. Chem. A* **103**, 2321 (1999).
- ²³G. J. Atchity, S. S. Xantheas, and K. Ruedenberg, *J. Chem. Phys.* **95**, 1862 (1991).
- ²⁴B. O. Roos, P. R. Taylor, and P. E. M. Siegbahn, *Chem. Phys.* **48**, 157 (1980).
- ²⁵B. O. Roos, in *Advances in Chemical Physics: Ab Initio Methods in Quantum Chemistry—II*, edited by K. P. Lawley (Wiley, Chichester, 1987), Vol. LXIX, p. 399.
- ²⁶M. W. Schmidt and M. S. Gordon, *Annu. Rev. Phys. Chem.* **49**, 233 (1998).
- ²⁷T. H. Dunning, Jr., *J. Chem. Phys.* **90**, 1007 (1989).
- ²⁸K. Andersson, P.-A. Malmqvist, and B. O. Roos, *J. Chem. Phys.* **96**, 1218 (1992).

- ²⁹MOLCAS 4.1 program. K. Andersson, M. R. A. Blomberg, M. P. Fülscher *et al.*, Lund University, Sweden, 1998.
- ³⁰W. C. Ermler, H. C. Hsieh, and L. B. Harding, *Comput. Phys. Commun.* **51**, 257 (1988).
- ³¹E02 and E04 subroutines from the NAG Fortran Library Mark 15. The Numerical Algorithms Group Ltd., Oxford, UK.
- ³²M. J. Frisch, G. W. Trucks, H. B. Schlegel *et al.*, GAUSSIAN 98, Revision A.7, Gaussian, Inc., Pittsburgh, PA, 1998.
- ³³M. González, R. Valero, and R. Sayós, *J. Chem. Phys.* **113**, 10983 (2000).
- ³⁴M. González, I. Miquel, and R. Sayós, *Chem. Phys. Lett.* **335**, 339 (2001).
- ³⁵R. Jost, J. Nygård, A. Pasinski, and A. Delon, *J. Chem. Phys.* **105**, 1287 (1996).
- ³⁶X. Landolt-Börnstein, in *Structure Data of Free Polyatomic Molecules*, edited by W. Martienssen (Springer-Verlag, Berlin, 1998), Vol. II/25A.
- ³⁷R. Georges, Doctoral thesis, Université Joseph Fourier, Grenoble, 1994.
- ³⁸J. L. Hardwick and J. C. D. Brand, *Chem. Phys. Lett.* **21**, 458 (1973).
- ³⁹J. L. Hardwick and J. C. D. Brand, *Can. J. Phys.* **54**, 80 (1976).
- ⁴⁰G. Herzberg, *Molecular Spectra and Molecular Structure. Vol. III. Electronic Spectra and Electronic Structure of Polyatomic Molecules* (Van Nostrand, New York, 1966).
- ⁴¹E. R. Davidson, *J. Am. Chem. Soc.* **99**, 397 (1977).
- ⁴²J. Katriel and E. R. Davidson, *Chem. Phys. Lett.* **76**, 259 (1980).
- ⁴³J. Finley, P.-Å. Malmqvist, B. O. Roos, and L. Serrano-Andrés, *Chem. Phys. Lett.* **288**, 299 (1998).
- ⁴⁴M. J. Beapark, M. A. Robb, and H. B. Schlegel, *Chem. Phys. Lett.* **223**, 269 (1994).
- ⁴⁵I. N. Ragazos, M. A. Robb, F. Bernardi, and M. Olivucci, *Chem. Phys. Lett.* **197**, 217 (1992).
- ⁴⁶G. Hirsch, R. J. Buenker, and C. Petrongolo, *Mol. Phys.* **76**, 1261 (1992).
- ⁴⁷R. Sayós, C. Oliva, and M. González, *J. Chem. Phys.* **117**, 670 (2002), preceding paper.